Fast Solution-Combustion Synthesis of Nitrogen-Modified Li$_4$Ti$_5$O$_{12}$ Nanomaterials with Improved Electrochemical Performance

Xue Li, Huang-chang Lin, Wang-jun Cui, Qian Xiao, and Jin-bao Zhao*

State Key Laboratory of Physical Chemistry of Solid Surfaces, Collaborative Innovation Center of Chemistry for Energy Materials, Department of Chemistry, College of Chemistry and Chemical Engineering, Xiamen University, Xiamen 361005, China

Ⓢ *Supporting Information*

ABSTRACT: A series of nitrogen-modified Li$_4$Ti$_5$O$_{12}$ (N-LTO) nanomaterials with hierarchical micro/nanoporous structures are first synthesized via a facile one-step combustion process using thermal decomposition of urea. Successful deposition of a TiN thin layer onto the LTO surface was confirmed by transmission electron microscopy with energy-dispersive X-ray analysis, X-ray photoelectron spectroscopy, Raman spectroscopy, and thermogravimetric measurements. The electrochemical performances of the N-LTO nanomaterials are also investigated in this work. Compared with pristine LTO, the N-LTO nanomaterial with 1.1 wt % nitrogen exhibits a higher rate capability and better reversibility. At charge/discharge rates of 1, 2, 8, and 15 C, the discharge capacities of the N-LTO electrode were 159, 150, 128, and 108 mAh g^{-1}, respectively. After 200 cycles at 1 C, its capacity retention was 98.5% with almost no capacity fading.

KEYWORDS: lithium battery, anode electrode, decomposition of urea, deposition of TiN
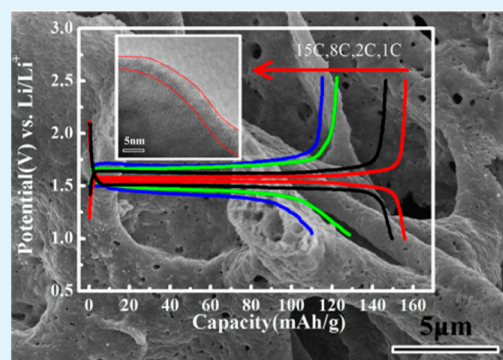
1. INTRODUCTION

Among currently available energy-storage technologies, the rechargeable lithium-ion battery (LIB) has received considerable attention from both the academic community and industry as a power source for hybrid electric vehicles (HEVs) and portable electronic devices because of its long cycle life and high energy density.[1−3] However, the deployment of large-scale LIBs for application in HEVs is significantly hindered by several major technological barriers, including insufficient cycle life, poor charge/discharge rate capability, and intrinsically poor safety characteristics.[4,5] Therefore, the search for electrode materials to meet these requirements is critical for large-scale battery development.

Compared with the commonly used graphitic carbon anode materials, spinel Li$_4$Ti$_5$O$_{12}$ (LTO) exhibits a flat and relatively high lithium insertion/extraction voltage at approximately 1.55 V (vs Li$^+$/Li), which is approximately 1.3 V higher than the operating voltage of graphitic anodes; thus, the formation of SEI layers and the electroplating of lithium can be avoided.[1,3,6,7] Moreover, as a zero-strain insertion material, LTO possesses excellent reversibility and lithium-ion mobility in the charge/discharge process.[8−10] In addition, spinel LTO has a high thermal stability, especially at elevated temperatures.[11] These features make it a promising anode material for large-scale and long-life energy-storage batteries. However, LTO has a poor electronic conductivity, approximately 10^{-13} S cm^{-1} because of empty Ti 3d states with a band gap energy of 2−3 eV,[12,13] which may give a moderate rate performance for high-power batteries. Moreover, LTO-based batteries will swell during the charge/discharge and storage processes, which is likely attributable to the generated gases (e.g., H$_2$, CO$_2$, and CO) originating from the interfacial reactions between LTO and the surrounding alkyl carbonate solvents.[14]

The most common strategies for improving the LTO electrochemical performance are (1) particle-size reduction to the nanometer scale to shorten the lithium-ion diffusion length,[15,16] (2) structural doping with metal or nonmetal ions in the lithium, titanium, or oxygen sites,[17−20] and (3) surface coating with electronic conductive materials to reduce the resistance.[21−23] However, the first two strategies cannot construct a barrier layer in suppressing the interfacial reaction and resulting gassing from the LTO surface. Meanwhile, some structure modifications (structural doping) will increase the existence of defects, which is detrimental: octahedral defects (16d) reduce the capacity, and tetrahedral defects (8a) generate an irreversible insertion capacity loss.[24] Therefore, constructing a conductive layer is seen as the most effective method to solve the main problems of the LTO battery. Currently, surface modification with nitrogen was demonstrated to be beneficial. Hu, Meng, Li, and Zhang et al. modified the surface structure of LTO with nitrogen-doped carbon coatings.[25−29] With the electron-conducting layer, the electrochemical performances of the LTO electrodes were substantially improved. It was found that nitrogen-doped carbon possesses many active defects, which are beneficial for Li$^+$ diffusion. Shen et. al developed a facile template-free route to fabricate Li$_4$Ti$_5$O$_{12}$ nanowire arrays

(LTO NWAs) growing directly on titanium foil and reported its electronic conductivity was enhanced by creating Ti^{3+} sites through hydrogenation.[30] Park et al. introduced thermal nitridation to LTO via annealing in NH_3. The authors attributed the significant enhancement in the battery performances to a mixed-valent intermediate phase, $Li_{4+\delta}Ti_5O_{12}$, and the surface conductive layer of TiN.[31]

Currently, most of the existing surface modification techniques require multistep [the first step is to synthesize LTO (the time consumption is at least 10 h), and the second step is to modify LTO with various nitrogen sources] and laborious procedures and are only applicable to certain substrates (such as nitrogen-doped carbon derived from pyridine and ionic liquid). In this regard, we report a facile, one-pot synthesis of nitrogen-modified LTO nanomaterials via combustion synthesis using thermal decomposition of urea. Compared with conventional coating methods, this route is easy to control, and there are some special advantages: (1) the one-step heating treatment may shorten the reaction time and reduce the energy cost, (2) combustion synthesis in the liquid phase ensures excellent product homogeneity with a high surface area,[32−34] and (3) as a nitrogen source, urea is inexpensive and safe to handle.[26,35] In addition, the thin surface layer of TiN enhances the electronic conductivity of the anode material, which leads to a greatly improved rate capability and cycle life.

2. EXPERIMENTAL SECTION

2.1. Material Synthesis. The pristine LTO nanopowders were prepared by solution−combustion synthesis using a titanyl nitrate [$TiO(NO_3)_2$] aqueous solution and $LiNO_3$ as the oxidant precursors and glycine as the fuel, with stoichiometric amounts of titanyl nitrate (0.0362 mol), 2.1 g of $LiNO_3$ (0.0303 mol), and 3.00 g of glycine (0.400 mol). Synthesis of the [$TiO(NO_3)_2$] aqueous solution is as follows. The transparent titanyl nitrate solution was prepared by adding nitric acid into $TiO(OH)_2$ under continuous stirring, which precipitated from the slow dropping of *tert*-butyl titanate [Ti-$(C_4H_9O)_4$] into dilute ammonia under an ice-water bath and vigorous stirring. A stoichiometric amount of $LiNO_3$ was then added to the solution, followed by the introduction of glycine as the fuel. Afterward, the mixture was placed in an alumina crucible and calcined in a muffle furnace in an argon atmosphere at 800 °C for 30 min after heating to 800 °C at a heating rate of 5 °C min^{-1}. When the temperature cooled to room temperature, the pristine LTO material was obtained. N-LTO nanomaterials were prepared via a similar route, but different amounts of urea (2.64, 3.96, and 5.35 g), placed in another alumina crucible to produce NH_3, were introduced during calcination. They are named as Nx-LTO, with x being the mass ratio of nitrogen, as identified by elemental analysis.

2.2. Material Characterization. The X-ray diffraction (XRD) patterns were recorded with a Philips X'pert Pro Super X-ray diffractometer and Cu Kα radiation. X-ray photoelectron spectroscopy (XPS) analysis was performed with a Quantum 2000 Scanning ESCA Microprobe spectrometer using focused monochromatized Al Kα radiation (1486.6 eV). The pass energy was 60 eV for the survey spectra and 20 eV for particular elements. The morphologies of the as-prepared materials were characterized by field-emission scanning electron microscopy (LEO 1530, Hitachi S-4800) and high-resolution transmission electron microscopy (HRTEM; Philips JEM-2100). The thermogravimetric (TG) measurements were conducted with a Rigaku Thermo Plus TG8120 system in an air atmosphere at a heating rate of 10 °C min^{-1} from room temperature to 800 °C. The content of nitrogen was measured by elemental analysis on a Vario Elemental III instrument (Elementar Co.). Raman spectra (Jobin Yvon Horiba Raman spectrometer model HR800) were collected by a 10 mW helium/neon laser at 632.8 nm excitation. The specific surface area of N1.1-LTO was measured by the Brunauer−Emmett−Teller (BET)

method using nitrogen adsorption−desorption isotherms on a Tristar 3000 system.

2.3. Electrochemical Measurements. Electrochemical evaluations were carried out by galvanostatic cycling of the electrodes, which were constructed with the as-prepared LTO samples in a CR2016-type coin cell. The working electrodes were formed by casting the slurry, composed of 80 wt % active materials, 10 wt % carbon black, and 10 wt % poly(vinylidene fluoride) dissolved in *N*-methylpyrrolidinone, onto an aluminum current collector foil. Afterward, the electrodes were dried under vacuum at 110 °C for 12 h (the electrode preparation process is the same, and the mass loading for the electrochemical test is controlled to about 3 mg cm^{-2}). The cells were assembled with the cathodes prepared as above and lithium metal as the anodes. The electrolytes contained a 1 mol L^{-1} $LiPF_6$ solution in a 1:1 (v:v) mixture of ethylene carbonate and dimethyl carbonate. All assembly processes of the test cells were carried out in an argon-filled glovebox. Galvanostatic charge/discharge experiments were performed at different current densities between 1.0 and 2.5 V (vs Li^+/Li) using a CT2001A cell test instrument (LAND Electronic Co.). The electrochemical impedance spectra (EIS) of the pristine and modified LTO charged at 1.55 V were measured in the frequency range of 10 mHz to 100 kHz using two-electrode coil cells with lithium metal as the counter electrode via an Autolab PGSTAT 101 cell test instrument. After the powder samples were pressed into disks at 20 MPa with an usual diameter of 12 mm and a typical thickness of 1 mm, a four-point probe meter [SX1934 (SZ-82) digital four-probe testing instrument] was used to measure the electronic conductivity of the samples.

3. RESULTS AND DISCUSSION

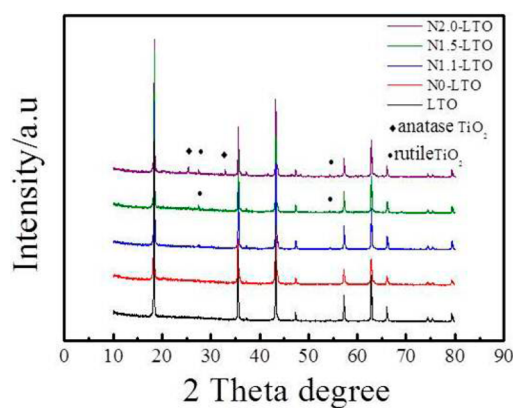The XRD patterns of the nitridated and pristine LTO nanomaterials are shown in Figure 1. The obtained materials

Figure 1. XRD patterns of nitridated and pristine LTO nanomaterials.

were named as Nx-LTO (x = mass percent of nitrogen), and the nitrogen content was confirmed by elemental analysis. Sharp diffraction peaks of the four samples signify good crystallization and can all be indexed to cubic spinel LTO (JCPDS No. 49-0207). After the thermal nitridation treatment, all of the Bragg reflections of the LTO phase remain intact except some impurity peaks, marked with symbols in Figure 1. The TiO_2 anatase ($2\theta = 25.2°$ and $32.7°$; JCPDS:00-021-1272) and TiO_2 rutile ($2\theta = 27.5°$ and $54.2°$; JCPDS:00-021-1276) phases appear with an increase of the nitrogen content, which may be due to the nitridation of LTO. A similar phenomenon has been reported,[31] but the specific reason for the changes is still not clear.·

After thermal nitridation at 800 °C, white LTO becomes discolored and is apparently brownish with 1.1 wt % N, as shown in Figure 2a. This discoloration is one of the direct
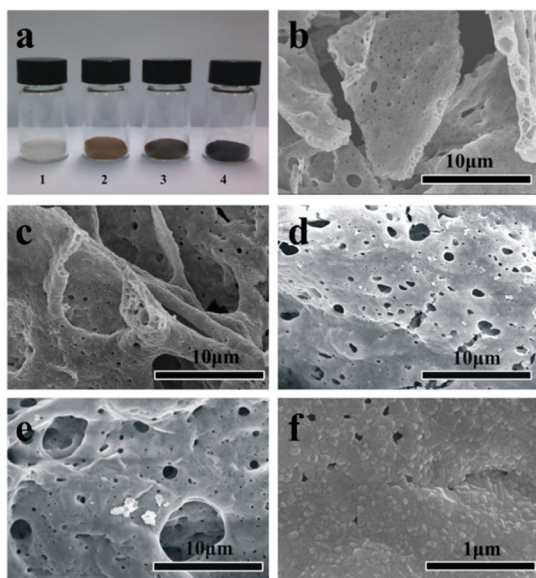
Figure 2. (a) Change in the color of the LTO powder before and after nitridation. Sample 1: N0-LTO. Sample 2: N1.1-LTO. Sample 3: N1.5-LTO. Sample 4: N2.0-LTO. SEM images of (b) N0-LTO, (c) N1.1-LTO, (d) N1.5-LTO, and (e) N2.0-LTO. (f) Magnified SEM image of N1.1-LTO.

indications of the incorporation of nitrogen atoms in the LTO structure. SEM structural studies of LTO and N-LTO are shown in Figure 2. All of the samples prepared via the combustion method show micrometer-sized secondary particles composed of nanometer-sized primary particles, which is optimal for practical usage as electrode materials. For the N-LTO samples, the sizes are uniform (Figure 2b) and are in a range of 50−100 nm (Figure 2f).

The electrochemical performance of N1.1-LTO is the best among these samples (discussed later); thus, we decided to examine it in more detail. Figure 3a reveals that it is composed
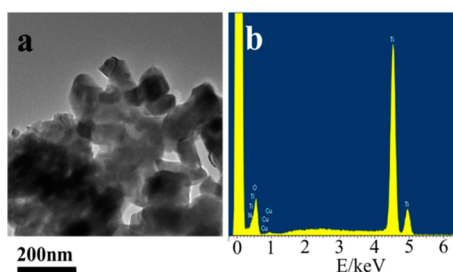

Figure 3. (a) TEM image of N1.1-LTO. (b) Corresponding surface EDS spectrum of part a.

of nanoparticles with diameters of approximately 100 nm. Figure 3b shows the energy-dispersive spectrometry (EDS) spectrum of the N1.1-LTO nanoparticles; the average mass percent of nitrogen is calculated to be approximately 1.1 wt %. We also make use of BET analysis to obtain more surface information on the N1.1-LTO sample. It was found that the BET surface area of N1.1-LTO was 8 m^2 g^{-1} (Figure S1 in the Supporting Information, SI) and the averaged pore volume observed for the sample using the Barrett−Joyner−Halenda method is 2×10^{-2} cm^3 g^{-1}. However, the macroporosity could not be measured because the macropores are too large to observe by a nitrogen adsorption method.[36]

To understand why nitridation improves the LTO performance and the surface structure of nitridized LTO nanoparticles, the N1.1-LTO sample was investigated by HR-TEM and surface EDS, as seen in Figure 4. It is clearly observed that a
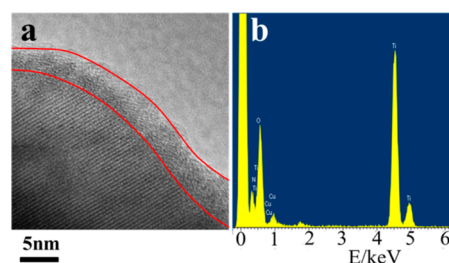

Figure 4. (a) HR-TEM image and (b) the corresponding surface EDS spectrum of N1.1-LTO.

thin shell with a thickness of approximately 5 nm was formed on the surface of the LTO nanocrystals from thermal decomposition of urea (Figure 4a). The nitrogen content of the shell in Figure 4a), as measured using EDS analysis (Figure 4b), is 8.5 wt %, which is considerably greater than the average mass ratio of nitrogen in the N1.1-LTO material. More HR-TEM images and the corresponding EDS analysis are shown in Figure S2 in the SI. It is clearly seen that a thin shell with a thickness of approximately 5 nm formed on the surface of the LTO nanocrystals from thermal decomposition of urea. EDS analysis showed, furthermore, that the nitrogen contents of the shell are 10.8 and 7.9 wt %, respectively. Compared with the results from elemental analysis (1.1 wt %) and TEM in the previous paragraph, the thin shell layer is rich in nitrogen.

Raman spectroscopy is an effective method to characterize the functional groups on the nanocrystal surface. Figure 5
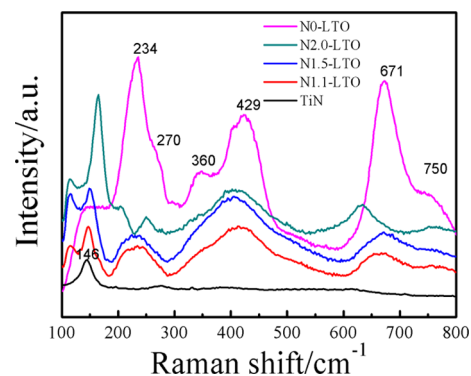

Figure 5. Raman spectra of pristine LTO, N-LTO, and TiN.

shows the Raman spectra of N-LTO and TiN (99 wt %, purchased from Sigma Co.). In the N0-LTO sample, the spectrum shows a good agreement with that reported in the literature,[37,38] where the peaks at 671 and 750 cm^{-1} are attributed to vibrations of the Ti−O bonds in octahedral TiO$_6$. The bending vibration of the O−Ti−O angle is observed at 234 cm^{-1}. The frequency lines at 429 and 360 cm^{-1} correspond to the stretching vibrations of the Li−O bonds in LiO$_4$ and polyhedral LiO$_6$. In addition to the Raman-allowed peaks of LTO, a new peak is observed at a lower frequency (146 cm^{-1}) in the spectra of the N-LTO materials, which is assigned to the TA mode of TiN,[39] enhanced by the increased nitrogen content. The above results clearly show that the nitridation of

LTO materials via thermal decomposition of urea can be carried out successfully.

XPS spectra of the N0-LTO and N-LTO materials are shown in Figure 6a. It can be clearly observed that a new peak at
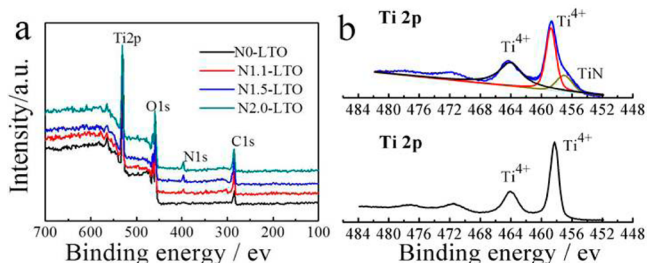

Figure 6. (a) XPS spectra of pristine LTO and N-LTO. (b) XPS analysis of Ti $2p_{3/2-1/2}$ for N1.1-LTO and N0-LTO.

approximately 397 eV, ascribed to N 1s, appears in the N-LTO samples, and its intensity increases with a stronger intensity of nitridation.[40,41] This result further suggests the presence of nitrogen in the N-LTO samples. The XPS Ti 2p peaks corresponding to LTO show a unique doublet at 458.8−464.4 eV, associated with tetravalent titanium based on $Ti^{+4}O_2$.[42,43] Compared with pristine LTO, we observe a new Ti 2p doublet at lower binding energies (455.8−461.9 eV) in the N1.1-LTO material (Figure 6b) after nitridation, which is assigned to the presence of trivalent titanium based on $Ti^{3+}N$.[42,43] The presence of a small amount of titanium oxynitrite (TiN_xO_y) cannot be excluded in this case. From a careful peak separation based on tetravalent and trivalent titanium, it is found that N1.1-LTO is composed of both TiN (5.4 wt %) and LTO (94.6 wt %).

It is well-known that the oxidation reaction of TiN to TiO_2 occurs at a wide range of temperatures in air;[44,45] we can calculate the reaction rate from the mass gain based on eq 1.

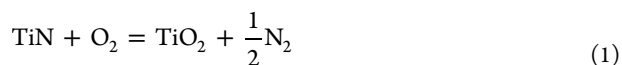$$TiN + O_2 = TiO_2 + \frac{1}{2}N_2 \qquad (1)$$

Figure 7 shows the TG curves of N0-LTO, N1.1-LTO, and pristine TiN in an air atmosphere. The weight increase of pure
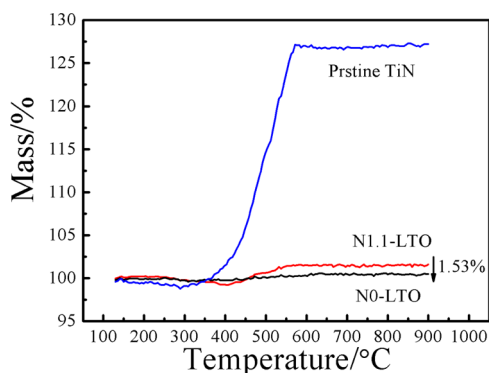

Figure 7. TG curves of N0-LTO, N1.1-LTO, and pure TiN in air.

TiN is due to the oxidation reaction of TiN to TiO_2, while there is no weight change in N0-LTO. In the case of N1.1-LTO, a weight increase of approximately 1.53% was observed. According to the equation, the nitrogen content of N1.1-LTO is calculated to be 1.17 wt %, which agrees well with the results from our other analyses (see Table 1), except that from XPS.

Table 1. Content (in Weight Percent) of Nitrogen and TiN in the Nitrogen-Modified LTO Samples Obtained via Different Test Methods

	EDS		elem anal.		XPS		TG	
	N	TiN	N	TiN	N	TiN	N	TiN
N1.1-LTO	1.1	5.0	1.1	5.0	1.2	5.3	1.2	5.3

The contents of nitrogen and TiN in the N-LTO samples as measured via different analysis methods are summarized in Table 1. The EDS and elemental analysis results show the same mass ratio of nitrogen and TiN to be 1.1 and 5.0 wt %, respectively. To further investigate the nitrogen content, XPS and TG analyses were performed, and the mass ratios of nitrogen and TiN were determined to be 1.2 and 5.3 wt %, respectively. Compared with quantitative analysis via elemental analysis, the measured results of the other three methods are consistent. These results further prove that this surface modification is effective and the presence of nitrogen is uniform.

Figure 8a shows a comparison of the rate capabilities between N-LTO and pristine LTO electrodes at different current rates, each sustained for 5 cycles. The N1.1-LTO and N1.5-LTO electrodes show considerably higher reversible capacities than the N0-LTO electrode at all rates, and both samples reach nearly the same reversible capacities at low discharge/charge current rates. However, at a higher current rate, such as 15 C, the N1.1-LTO electrode shows a considerably higher reversible capacity (110 mAh g^{-1}), whereas the N1.5-LTO electrode achieves a capacity of 95 mAh g^{-1} at the same rate. However, the N2.0-LTO electrode shows no significant improvement compared with the N0-LTO electrode, which may be due to the large content of rutile and anatase TiO_2 impurities.[46,47] Overall, the N1.1-LTO electrode exhibits the best electrochemical performance, and another study has come to a similar conclusion.[31] A detailed comparison of the rate capabilities of the N0-LTO electrode with those of the N1.1-LTO electrode is shown in Figure 8b. As shown in Figure 8b, the N1.1-LTO electrode clearly exhibits a much higher storage capacity and a much better rate capability than the N0-LTO electrode. For instance, at a discharge and charge rate of 15 C, the specific capacity of the N1.1-LTO electrode is approximately 110 mAh g^{-1}, which is remarkably higher than the rate capacity (74 mAh g^{-1}) of the N0-LTO electrode.

Figure 9 presents the voltage profiles of the N0-LTO, N1.1-LTO, N1.5-LTO, and N2.0-LTO electrodes at the current rates of 1−15 C over a potential window of 1.0−2.5 V. At the initial lower rate of 1 C, the N1.1-LTO electrode shows a flat voltage plateau at a potential of 1.55 V and exhibits a discharge capacity of 159 mAh g^{-1}. As the current rate increased from 2 to 8 and then 15 C, the discharge capacity decreased gradually from 150 to 128 and then 108 mAh g^{-1}, respectively (Figure 9a). Compared to the N1.1-LTO electrode, the N0-LTO, N1.5-LTO, and N2.0-LTO electrodes not only show stronger polarization but also deliver a much lower storage capacity (Figure 9b).

A comparison of the voltage profiles for the prepared N1.1-LTO and N0-LTO electrodes is shown in Figure 10a. At a low current rate of 1 C, the polarization between the discharge and charge plateaus is 41 mV for N1.1-LTO, which is significantly lower than that for N0-LTO (78 mV). The lower polarization for the N1.1-LTO electrode is attributed to better reaction kinetics, which indicates improved electrical conductivity after
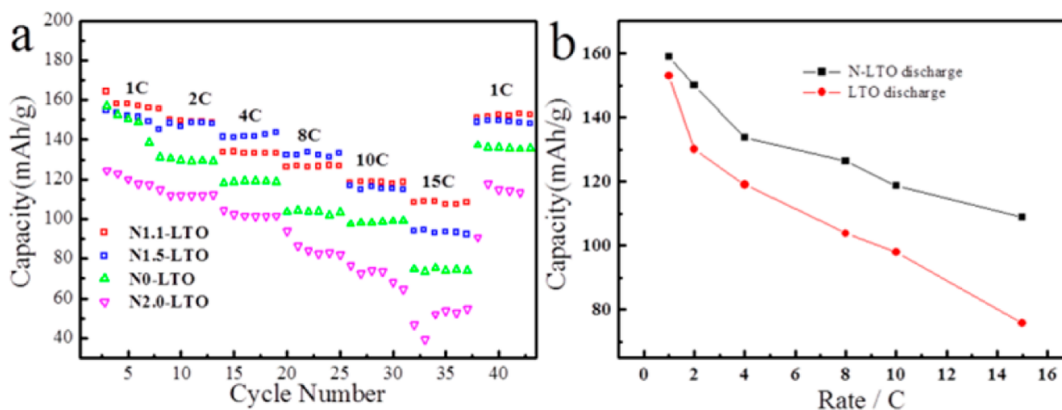
7898

dx.doi.org/10.1021/am501220f | ACS Appl. Mater. Interfaces 2014, 6, 7895−7901

Figure 8. (a) Charge capacities and rate capabilities of the prepared N-LTO materials and pristine LTO at different current densities. (b) Comparison of the rate capacity retention of N1.1-LTO and N0-LTO (data from the second circle at different rates).
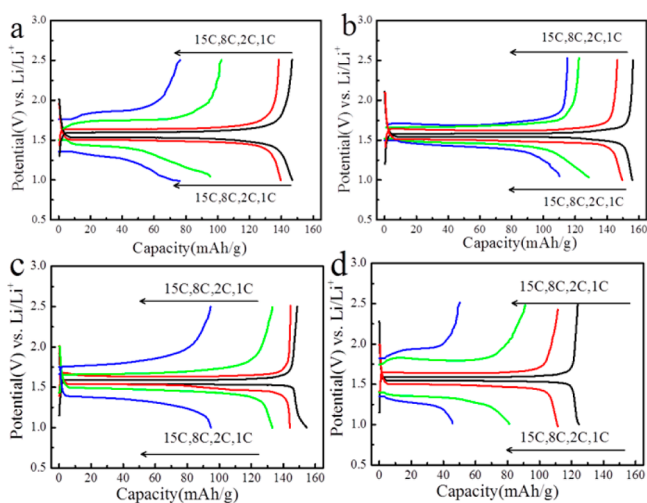

Figure 9. (a) Voltage profiles of N1.1-LTO and (b) N0-LTO, (c) N1.1-LTO, and (d) N2.0-LTO at different current rates (data from the second circle at different rates).

nitrogen modification. The cycling performances of the pristine and nitrogen-modified samples at 1 C in a half-cell are shown in Figure 10b. For the N0-LTO sample, the initial capacity is 152.1 mAh g^{-1}, and it decreases to 134.6 mAh g^{-1} after 200 cycles with a capacity retention of 88.5%. In the case of the N1.1-LTO sample, it delivers 159.1 mAh g^{-1} with a capacity retention of 98.5% after 200 cycles, demonstrating remarkable cycling stability. We also tested the cycling performance at 60 °C of the pure sample and N1.1-LTO at 1 C in coin cells. As

shown in Figure S3 in theSI, both electrodes show higher capacity (close to the theoretical capacity) than that at room temperature because of the faster lithium-ion transmission at high temperature. Compared with pristine LTO, N1.1-LTO showed slightly higher discharge capacity. After 150 cycles, the discharge capacities for pure LTO and N1.1-LTO were 125 and 150 mAh g^{-1}, respectively. This further shows the advantages of nitrogen modification for LTO materials.

To gain more information on the electrode kinetics, impedance spectra were recorded on the N1.1-LTO and N0-LTO half-cells. The impedance data and fitting using an equivalent circuit are shown in Figure 11. In this equivalent circuit, R_s and R_{ct} are the solution resistance and charge-transfer resistance, respectively. CPE represents the double-layer capacitance and passivation film capacitance. W represents the Warburg impedance.[48,49] Both EIS diagrams are composed of a depressed semicircle at high frequencies and a spike at low frequencies. The high-frequency semicircle is related to the charge-transfer resistance, while the spike at the low-frequency end indicates the Warburg impedance of long-range lithium-ion diffusion.[50] A good agreement was observed between the impedance data and fitting using the above-mentioned equivalent circuit model (the error is less than 5%). The parameters of the equivalent circuit are recorded in Table 2. Clearly, the N1.1-LTO electrode exhibits a much lower charge-transfer resistance than the N0-LTO electrode, confirming that nitrogen modification of the LTO material improves the electrical conductivity. At the same time, the electronic conductivity was measured by a four-point probe method. The test results show that the electronic conductivity of N1.1-
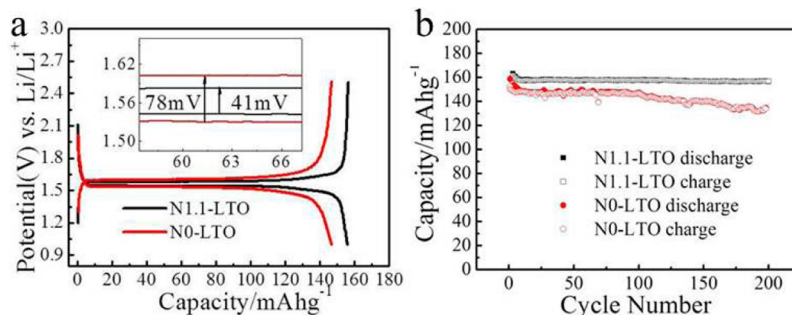

Figure 10. Electrochemical properties of the prepared N1.1-LTO and N0-LTO materials: (a) initial voltage profiles at 1 C; (b) specific capacity for 200 cycles at a rate of 1 C.
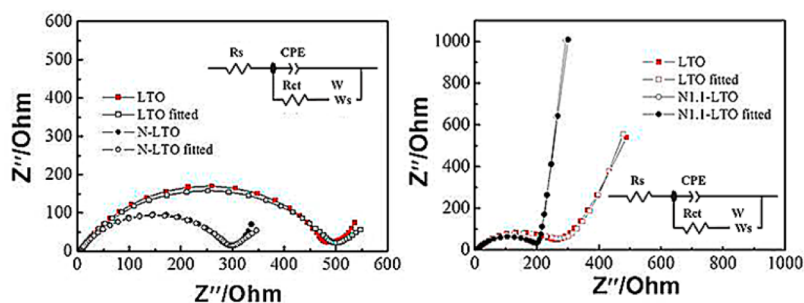
7899

dx.doi.org/10.1021/am501220f | ACS Appl. Mater. Interfaces 2014, 6, 7895−7901

Figure 11. (a) Alternating-current (ac) impedance measurements of the N1.1-LTO and N0-LTO electrodes at an open-circuit potential of ~3.0 V vs Li/Li$^+$. (b) ac impedance measurements of the N1.1-LTO and N0-LTO electrodes at a half discharge state of ~1.55 V vs Li/Li$^+$. The insets show the equivalent circuits for the EIS measurements.

Table 2. Impedance Parameters of the N1.1-LTO and N0-LTO Electrodes

	R_s (Ω)	error %	R_{ct} (Ω)	error %
N0-LTO (OCP)	8.0	4.7	270.5	2.2
N1.1-LTO (OCP)	7.4	3.6	202.8	2.2
N0-LTO (1.55 V)	6.5	2.2	487.8	1.2
N1.1-LTO (1.55 V)	6.2	2.8	286.9	1.0

LTO is 2.1×10^{-6} S cm^{-1} and that of pure LTO is 7.9×10^{-8} S cm^{-1}. On the basis of these findings, we do believe that the electrical conductivity can be improved via nitrogen modification.

4. CONCLUSION

In summary, we have first reported an efficient approach to preparing N-LTO nanomaterials in one step. When being evaluated as an anode material for LIBs, the N-LTO electrodes exhibit high rate capabilities and high stabilities for lithium storage. At a rate of 15 C, the N1.1-LTO electrode shows a discharge capacity of 108 mAh g^{-1} with a retention as high as 67.9%. In addition, after 200 cycles at 1 C, the capacity retention is as high as 98.5% with nearly no capacity fading. The superior electrochemical performance of N1.1-LTO was attributed to the LTO nanoparticles with a porous structure and nitrogen modification, which enabled faster ion transport and better electron conductivity. This surface modification is relatively simple and inexpensive and may be a helpful approach to solving the problems of poor electronic conductivity and rate performance. We believe that such a nitrogen surface modification method could be applied in a wide range of fields and that N-LTO could be a promising anode material for high-rate LIBs.

■ ASSOCIATED CONTENT

Ⓢ Supporting Information

Nitrogen adsorption−desorption isotherms at 77 K of N1.1-LTO, TEM images of N1.1-LTO and the corresponding surface EDS spectra, and cycling performance of the prepared N1.1-LTO and N0-LTO materials at 1 C at 60 °C. This material is available free of charge via the Internet at http://pubs.acs.org.

■ AUTHOR INFORMATION

Corresponding Author

*E-mail: jbzhao@xmu.edu.cn.

Notes

The authors declare no competing financial interest.

■ ACKNOWLEDGMENTS

■ REFERENCES

(1) Ohzuku, T.; Ueda, A.; Yamamoto, N. Zero-Strain Insertion Material of Li[Li$_{1/3}$Ti$_{5/3}$]O$_4$ for Rechargeable Lithium Cells. *J. Electrochem. Soc.* **1995**, *142*, 1431−1435.

(2) Armand, M.; Tarascon, J. M. Building better batteries. *Nature* **2008**, *451*, 652−657.

(3) Bruce, P. G.; Scrosati, B.; Tarascon, J. M. Nanomaterials for Rechargeable Lithium Batteries. *Angew. Chem., Int. Ed.* **2008**, *47*, 2930−2946.

(4) Shen, L. F.; Li, H. S.; Uchaker, E.; Zhang, X. G.; Cao, G. Z. General Strategy for Designing Core−Shell Nanostructured Materials for High-Power Lithium Ion Batteries. *Nano Lett.* **2012**, *12*, 5673−5678.

(5) Kang, E.; Jung, Y. S.; Cavanagh, A. S.; Kim, G. H.; George, S. M.; Dillon, A. C.; Kim, J. K.; Lee, J. Fe$_3$O$_4$ Nanoparticles Confined in Mesocellular Carbon Foam for High Performance Anode Materials for Lithium-Ion Batteries. *Adv. Funct. Mater.* **2011**, *21*, 2430−2438.

(6) Chen, Z. H.; Belharouak, I.; Sun, Y. K.; Amine, K. Titanium-Based Anode Materials for Safe Lithium-Ion Batteries. *Adv. Funct. Mater.* **2013**, *23*, 959−969.

(7) Young, D.; Ransil, A.; Amin, R.; Li, Z.; Chiang, Y. M. Electronic Conductivity in the Li$_{4/3}$Ti$_{5/3}$O$_4$−Li$_{7/3}$Ti$_{5/3}$O$_4$ System and Variation with State-of-Charge as a Li Battery Anode. *Adv. Energy Mater.* **2013**, *3*, 1125−1129.

(8) Shen, L. F.; Yuan, C. Z.; Luo, H. J.; Zhang, X. G.; Chen, L.; Li, H. S. Novel Template-Free Solvothermal Synthesis of Mesoporous Li$_4$Ti$_5$O$_{12}$-C Microspheres for High Power Lithium Ion Batteries. *J. Mater. Chem.* **2011**, *21*, 14414−14416.

(9) Thackeray, M. M. Structural Considerations of Layered and Spinel Lithiated Oxides for Lithium ion Batteries. *J. Electrochem Soc.* **1995**, *142*, 2558−2563.

(10) Aldon, L.; Kubiak, P.; Womes, M.; Jumas, J. C.; Olivier-Fourcade, J.; Tirado, J. L.; Corredor, J. I.; Vicente, C. P. Chemical and Electrochemical Li-Insertion into the Li$_4$Ti$_5$O$_{12}$ Spinel. *J. Chem. Mater.* **2004**, *16*, 5721−5725.

(11) Yi, T. F.; Xie, Y.; Zhu, Y. R.; Zhu, R. S.; Shen, H. Y. Structural and Thermodynamic Stability of Li$_4$Ti$_5$O$_{12}$ Anode Material for Lithium-Ion Battery. *J. Power Sources* **2013**, *222*, 448−454.

(12) Prosini, P. P.; Mancini, R.; Petrucci, L.; Contini, V.; Villano, P. Li$_4$Ti$_5$O$_{12}$ as Anode in All-Solid-State, Plastic, Lithium-ion Batteries for Low-power Applications. *Solid State Ionics* **2001**, *144*, 185−192.

7900

dx.doi.org/10.1021/am501220f | ACS Appl. Mater. Interfaces 2014, 6, 7895−7901

(13) Cheng, L.; Li, X. L.; Liu, H. J.; Xiong, H. M.; Zhang, P. W.; Xia, Y. Y. Carbon-Coated $Li_4Ti_5O_{12}$ as a High Rate Electrode Material for Li-Ion Intercalation. *J. Electrochem. Soc.* **2007**, *154*, A692–A697.

(14) He, Y. B.; Li, B. H.; Liu, M.; Zhang, C.; Lv, W.; Yang, C.; Li, J.; Du, H. D.; Zhang, B.; Yang, Q. H.; Kim, J. K.; Kang, F. Y. Gassing in $Li_4Ti_5O_{12}$-Based Batteries and Its Remedy. *Sci. Rep.* **2012**, *2*, 913–921.

(15) Chen, J. Z.; Yang, L.; Fang, S. H.; Hirano, S. I.; Tachibana, K. Synthesis of Hierarchical Mesoporous Nest-Like $Li_4Ti_5O_{12}$ for High-Rate Lithium Ion Batteries. *J. Power Sources* **2012**, *200*, 59–66.

(16) Feckl, J. M.; Fominykh, K.; Dcblinger, M.; Fattakhova-Rohlfing, D.; Bein, T. Nanoscale Porous Framework of Lithium Titanate for Ultrafast Lithium Insertion. *Angew. Chem.* **2012**, *51*, 7459–7463.

(17) Chen, C. H.; Vaughey, J. T.; Jansen, A. N.; Dees, D. W.; Kahaian, A. J.; Goacher, T.; Thackeray, M. M. Studies of Mg-Substituted $Li_{4-x}Mg_xTi_5O_{12}$ Spinel Electrodes ($0 \leqslant x \leqslant 1$) for Lithium Batteries. *J. Electrochem. Soc.* **2001**, *148*, A102–A104.

(18) Zhong, Z. Electrochem Synthesis of Mo^{4+} Substituted Spinel $Li_4Ti_{5-x}Mo_xO_{12}$. *Solid-State Lett.* **2007**, *10*, A267–A269.

(19) Yi, T. F.; Shu, J.; Zhu, Y. R.; Zhu, X. D.; Yue, C. B.; Zhou, A. N.; Zhu, R. S. High-Performance $Li_4Ti_{5-x}V_xO_{12}$ ($0 \leqslant x \leqslant 0.3$) as an Anode Material for Secondary Lithium-Ion battery. *Electrochim. Acta* **2009**, *54*, 7464–7470.

(20) Huang, S.; Wen, Z.; Gu, Z.; Zhu, X. Preparation and Cycling Performance of Al^{3+} and F^- Co-Substituted Compounds $Li_4Al_xTi_{5-x}F_yO_{12-y}$. *Electrochim. Acta* **2005**, *50*, 4057–4062.

(21) Zhu, G. N.; Liu, H. J.; Zhuang, J. H.; Wang, C. X.; Wang, Y. G.; Xia, Y. Y. Carbon-Coated Nano-Sized $Li_4Ti_5O_{12}$ Nanoporous Micro-Sphere as Anode Material for High-Rate Lithium-Ion Batteries. *Energy Environ. Sci.* **2011**, *4*, 4016–4022.

(22) Huang, S. H.; Wen, Z. Y.; Lin, B.; Han, J. D.; Xu, X. G. The High-Rate Performance of the Newly Designed $Li_4Ti_5O_{12}/Cu$ Composite Anode for Lithium Ion Batteries. *J. Alloys Compd.* **2008**, *457*, 400–403.

(23) Jung, H. G.; Myung, S. T.; Yoon, C. S.; Son, S. B.; Oh, K. H.; Amine, K.; Scrosati, B.; Sun, Y. K. Microscale Spherical Carbon-Coated $Li_4Ti_5O_{12}$ as Ultra High Power Anode Material for Lithium Batteries. *Energy Environ. Sci.* **2011**, *4*, 1345–1351.

(24) Kubiak, P.; Garcia, A.; Womes, M.; Aldon, L.; Fourcade, J. O.; Lippens, P. E.; Jumas, J. C. Phase Transition in the Spinel $Li_4Ti_5O_{12}$ Induced by Lithium Insertion - Influence of the Substitutions Ti/V, Ti/Mn, Ti/Fe. *J. Power Sources* **2003**, *119*, 626–630.

(25) Zhao, L.; Hu, Y. S.; Li, H.; Wang, Z. X.; Chen, L. Q. Porous $Li_4Ti_5O_{12}$ Coated with N-Doped Carbon from Ionic Liquids for Li-Ion Batteries. *Adv. Mater.* **2011**, *23*, 1385–1388.

(26) Pan, H.; Zhao, L.; Hu, Y. S.; Li, H.; Chen, L. Q. Improved Li-Storage Performance of $Li_4Ti_5O_{12}$ Coated with CN Compounds Derived from Pyrolysis of Urea through a Low-Temperature Approach. *ChemSusChem* **2012**, *5*, 526–529.

(27) Ding, Z. J.; Zhao, L.; Suo, L. M.; Jiao, Y.; Meng, S.; Hu, Y. S.; Wang, Z. X.; Chen, L. Q. Towards Understanding the Effects of Carbon and Nitrogen-Doped Carbon Coating on the Electrochemical Performance of $Li_4Ti_5O_{12}$ in Lithium Ion Batteries: a Combined Experimental and Theoretical Study. *Phys. Chem. Chem. Phys.* **2011**, *13*, 15127–15133.

(28) Li, H. S.; Shen, L. F.; Zhang, X. G.; Wang, J.; Nie, P.; Che, Q.; Ding, B. Nitrogen-Doped Carbon Coated $Li_4Ti_5O_{12}$ Nanocomposite: Superior Anode Materials for Rechargeable Lithium Ion Batteries. *J. Power Sources* **2013**, *221*, 122–127.

(29) Zhang, H. Q.; Deng, Q. J.; Mou, C. X.; Huang, Z. L.; Wang, Y.; Zhou, A. J.; Li, J. Z. Surface Structure and High-Rate Performance of Spinel $Li_4Ti_5O_{12}$ Coated with N-Doped Carbon as Anode Material for Lithium-Ion Batteries. *J. Power Sources* **2013**, *239*, 538–545.

(30) Shen, L. F.; Uchaker, E.; Zhang, X. G.; Cao, G. Z. Hydrogenated $Li_4Ti_5O_{12}$ Nanowire Arrays for High Rate Lithium Ion Batteries. *Adv. Mater.* **2012**, *24*, 6502–6506.

(31) Park, K. S.; Benayad, A.; Kang, D. J.; Doo, S. G. Nitridation-Driven Conductive $Li_4Ti_5O_{12}$ for Lithium Ion Batteries. *J. Am. Chem. Soc.* **2008**, *130*, 14930–14931.

(32) Yuan, T.; Wang, K.; Cai, R.; Ran, R.; Shao, Z. P. Cellulose-Assisted Combustion Synthesis of $Li_4Ti_5O_{12}$ Adopting Anatase TiO_2 Solid as Raw Material with High Electrochemical Performance. *J. Alloys Compd.* **2009**, *477*, 665–672.

(33) Raja, M. W.; Mahanty, S.; Kundu, M.; Basu, R. N. Synthesis of Nanocrystalline $Li_4Ti_5O_{12}$ by a Novel Aqueous Combustion Technique. *J. Alloys Compd.* **2009**, *468*, 258–267.

(34) Prakash, A. S.; Manikandan, P.; Ramesha, K.; Sathiya, M.; Tarascon, J. M.; Shukla, A. K. Solution-Combustion Synthesized Nanocrystalline $Li_4Ti_5O_{12}$ as High-Rate Performance Li-Ion Battery Anode. *Chem. Mater.* **2010**, *22*, 2857–2863.

(35) Yim, S. D.; Kim, S. J.; Baik, J. H.; Nam, I. S.; Mok, Y. S.; Lee, J. H.; Cho, B. K.; Oh, S. H. Decomposition of Urea into NH_3 for the SCR Process. *Chem. Res.* **2004**, *43*, 4856–4863.

(36) Gregy, S. J.; Sing, K. S. *Adsoption surface area and porosity*, 2nd ed.; Academic Press: London, 1982; Vol. 6, pp 24–27.

(37) Taberna, P. L.; Mitra, S.; Poizot, P.; Simon, P.; Tarascon, J. M. High Rate Capabilities Fe_3O_4-Based Cu Nano-Architectured Electrodes for Lithium-Ion Battery Applications. *Nat. Mater.* **2006**, *5*, 567–573.

(38) Wang, D. H.; Choi, D. W.; Li, J.; Yang, Z. G.; Nie, Z. M.; Kou, R.; Hu, D. H.; Wang, C. M.; Saraf, L. V.; Zhang, J. G.; Aksay, I. A.; Liu, J. Self-Assembled TiO_2–Graphene Hybrid Nanostructures for Enhanced Li-Ion Insertion. *ACS Nano* **2009**, *3*, 907–914.

(39) Chin, Z. H.; Perng, T. P. In Situ Observation of Combustion to Form TiN During Ball Milling Ti in Nitrogen. *Appl. Phys. Lett.* **1997**, *70*, 2380–2382.

(40) Valentin, C. D.; Pacchioni, G.; Selloni, A.; Livraghi, S.; Giamello, E. Characterization of Paramagnetic Species in N-Doped TiO_2 Powders by EPR Spectroscopy and DFT Calculations. *J. Phys. Chem. B* **2005**, *109*, 11414–11419.

(41) Saha, N. C.; Tompkins, H. G. Titanium Nitride Oxidation Chemistry: An X-ray Photoelectron Spectroscopy Study. *J. Appl. Phys.* **1992**, *72*, 3072–3079.

(42) Jung, H. G.; Myung, S. T.; Yoon, C. S.; Son, S. B.; Oh, K. H.; Amine, K.; Scrosatiag, B.; Sun, Y. K. Microscale Spherical Carbon-Coated $Li_4Ti_5O_{12}$ as Ultra High Power Anode Material for Lithium Batteries. *Energy Environ. Sci.* **2011**, *4*, 1345–1351.

(43) Wagner, C. D.; Riggs, W. M.; Davis, L. E.; Moulder, J. F.; Mullenberg, G. E. *Handbook of X-Ray Photoelectron Spectroscopy*, 1st ed.; Physics and Electronics Division, Perkin Elmer Corp.: Eden Prairie, MN, 1979; Vol. 6, pp 24–27.

(44) Ichimura, H.; Kawana, A. High-Temperature Oxidation of Ion-Plated TiN and TiAlN Films. *J. Mater. Res.* **1993**, *8* (5), 1093–1100.

(45) Gwo, S.; Yeh, C. L.; Chen, P. F.; Chou, Y. C.; Chen, T. T. Local Electric-Field-Induced Oxidation of Titanium Nitride Films. *Appl. Phys. Lett.* **1999**, *74*, 1090–1100.

(46) Wang, L.; Xiao, Q. Z.; Li, Z. H.; Lei, G. T.; Zhang, P.; Wu, L. J. Synthesis of $Li_4Ti_5O_{12}$ fibers as a high-rate electrode material for lithium-ion batteries. *J. Solid State Electrochem.* **2012**, *16*, 3307–3313.

(47) Xie, L. L.; Xu, Y. D.; Zhang, J.J.; Gao, X. Y.; Wang, B.; Yan, X. Y.; Qu, L.B. Facile Synthesis and Characterization of $Li_4Ti_5O_{12}$ as Anode Material for Lithium Ion Batteries. *Int. J. Electrochem. Sci.* **2013**, *8*, 1701–1712.

(48) Shenouda, A. Y.; Liu, H. K. Electrochemical Behaviour of Tin Borophosphate Negative Electrodes for Energy Storage Systems. *J. Power Sources* **2008**, *185*, 1386–1391.

(49) Shenouda, A. Y.; Murali, K. R. Electrochemical Properties of Doped Lithium Titanate Compounds and Their Performance in Lithium Rechargeable Batteries. *J. Power Sources* **2008**, *176*, 332–339.

(50) Schweikert, N.; Hahn, H.; Indris, S. Cycling Behaviour of Li/$Li_4Ti_5O_{12}$ Cells Studied by Electrochemical Impedance Spectroscopy. *Phys. Chem. Chem. Phys.* **2011**, *13*, 6234–6240.